

Article

Crystal Structure of Chaperonin *GroEL* from *Xanthomonas oryzae* pv. *oryzae*

Huyen-Thi Tran ^{1,†}, Jongha Lee ^{1,†}, Hyunjae Park ¹, Jeong-Gu Kim ², Seunghwan Kim ²,
Yeh-Jin Ahn ³ and Lin-Woo Kang ^{1,*} 

¹ Department of Biological Sciences, Konkuk University, 120 Neungdong-ro, Gwangjin-gu, Seoul 05029, Korea

² Genomics Division, National Institute of Agricultural Sciences, Rural Development Administration (RDA), Jeonju 03016, Korea

³ Department of Biotechnology, Sangmyung University, 20 Hongji-dong 2-gil, Jongno-gu, Seoul 03016, Korea

* Correspondence: lkang@konkuk.ac.kr; Tel.: +82-2-450-4090

† These authors contributed equally to this paper.

Received: 16 July 2019; Accepted: 28 July 2019; Published: 2 August 2019



Abstract: *Xanthomonas oryzae* pv. *oryzae* (*Xoo*) is a plant pathogen that causes bacterial blight of rice, with outbreaks occurring in most rice-growing countries. Thus far, there is no effective pesticide against bacterial blight. Chaperones in bacterial pathogens are important for the stabilization and delivery of effectors into host cells to cause disease. In bacteria, *GroEL*/*GroES* complex mediates protein folding and protects proteins against misfolding and aggregation caused by environmental stress. We determined the crystal structure of *GroEL* from *Xanthomonas oryzae* pv. *oryzae* (*XoGroEL*) at 3.2 Å resolution, which showed the open form of two conserved homoheptameric rings stacked back-to-back. In the open form structure, the apical domain of *XoGroEL* had a higher B factor than the intermediate and equatorial domains, indicating that the apical domain had a flexible conformation before the binding of substrate unfolded protein and ATP. The *XoGroEL* structure will be helpful in understanding the function and catalytic mechanism of bacterial chaperonin *GroELs*.

Keywords: *GroEL*; chaperonin; *Xanthomonas oryzae* pv. *oryzae* (*Xoo*); protein crystallography

1. Introduction

Rice is the most cultivated food crop, feeding more than half of the world population [1]. Although a rapidly growing global population has led to an increase in demand for rice, severe environment stresses, such as climate change and disease pressures, add challenges to rice production [2]. *Xanthomonas oryzae* pv. *oryzae* (*Xoo*) causes bacterial blight, which is one of the most problematic diseases in rice and can cause crop losses of up to 50% [3].

Type III secretion system (T3SS) encoded by *hrp* genes is essential for the pathogenicity of *Xoo*, via which virulent T3 effector proteins are delivered to rice to modulate the host system for disease progress [4]. The T3SS consists of a narrow, needle-like structure such as pili, within which T3 effectors should be translocated to host rice [5]. Chaperones in *Xoo* play a role in stabilizing effector proteins before the delivery to host [6,7].

Most proteins need assistance to fold into their native three-dimensional state to achieve correct functions [8]. In the extremely crowded cellular environment, newly synthesized proteins are prone to aggregate, and partially folded or unfolded proteins are toxic to life. Chaperonins have large, double-ring complexes of 800–1000 kDa with 7–9 subunits per ring [9]. Chaperonins are classified into two structural groups: Group I and Group II. *GroEL* in bacteria and heat-shock protein 60 (Hsp60) in eukaryotic organelles belong to Group I, while thermosome in archaea and chaperonin, such as TCP1 or TCP1 ring complex in eukaryotic cytosol, belong to Group II [9]. In this study, we determined the

crystal structure of *XoGroEL* at 3.2 Å resolution from the plant pathogen *Xoo*. The findings will be useful in understanding the allosteric protein folding machinery of *GroEL*.

2. Materials and Methods

2.1. Reagents

The expression vector, pET11a, was purchased from Novagen (San Diego, CA, USA). The expression host cell, *Escherichia coli* BL21 (DE3), and all restriction enzymes were purchased from New England Biolabs (Hertfordshire, UK). Luria-Bertani (LB) medium was purchased from BD Biosciences (San Jose, CA, USA). The prestained protein makers for SDS-PAGE were purchased from MBI Fermentas (Hanover, MD, USA).

2.2. Gene Cloning and Protein Expression and Purification

Gene cloning and protein expression and purification were performed as described in [10]. Basically, the *XoGroEL* (*Xoo4288*)-coding DNA sequence was amplified using the genomic DNA of *Xanthomonas oryzae* pv. *oryzae* (*Xoo ATCC10331*) as a template and cloned into a pET11a expression vector to generate the recombinant pET11a-His-TEV-*XoGroEL* plasmid, which harbors the *XoGroEL* gene with a 7×His tag at the N-terminus and a tobacco etch virus (TEV) protease cleavage site between the 7×His tag and *XoGroEL* gene.

The recombinant pET11a-His-TEV-*XoGroEL* plasmid was transformed into *E. coli* BL21(DE3) cells. Expression of *XoGroEL* was induced with 0.5 mM isopropyl β-D-1-thiogalactopyranoside (IPTG) at the optical density of 0.5 at 600 nm (OD₆₀₀). The induced cells were cultured for an additional 20 h at 288 K and harvested. The cell pellet was resuspended in a lysis buffer containing 25 mM Tris-HCl (pH 7.5), 250 mM NaCl, and 10 mM imidazole and homogenized on ice using ultrasonication (Sonomasher, S&T Science, South Korea). The crude cell extract was centrifuged at 277 K for 30 min at 21,000 × g (Vision VS24-SMTi V508A rotor) to remove cell debris. The lysate was applied onto a Ni-NTA His-Bind[®] Resin (Novagen) to purify *XoGroEL*. *XoGroEL* protein was eluted by an elution buffer containing 25 mM Tris-HCl (pH 7.5), 250 mM NaCl, and 250 mM imidazole. Dialyzed *XoGroEL* protein was loaded onto a 5 mL Hi-Trap Q FF column (GE Healthcare) equilibrated in buffer A containing 20 mM Tris-HCl (pH 8.0), 15 mM NaCl, and 3 mM β-mercaptoethanol. *XoGroEL* was washed and eluted with a gradient of 0%–100% buffer B (buffer A with 1 M NaCl). Purified *XoGroEL* was dialyzed against the crystallization buffer containing 20 mM Tris-HCl (pH 8.0), 20 mM NaCl, and 3 mM β-mercaptoethanol and concentrated to a final protein concentration of 7.8 mg mL⁻¹ with a Vivaspin20 concentrator (3000 MWCO, Satorius).

2.3. Crystallization and X-ray Data Collection

Initial crystallization was performed as described in [10]. Crystals of *XoGroEL* were obtained on a submicroliter scale at 287 K by the sitting-drop vapor-diffusion method in 96-well Intelli plates (Hampton Research) using a Hydra II e-drop automated pipetting system (Matrix). Thin crystals were observed in condition No. 1 of the Crystal Screen kit containing 0.02 M calcium chloride dihydrate, 0.1 M sodium acetate trihydrate (pH 4.6), and 30% (v/v) (+/-)-2-methyl-2,4 pentadiol. For the optimization of *XoGroEL* crystals, the hanging drops were manually set up with 0.7 μL of protein solution and 0.7 μL of reservoir solution in Nextal NCK-24 crystallization plates (Nextal Biotech, Canada) over 1 mL of reservoir solution. The initial crystallization reservoir solution was adjusted to the new solution containing 0.1 M sodium chloride dihydrate, 0.1 M sodium citrate (pH 4.0–4.5), and 25%–30% (v/v) (+/-)-2-methyl-2,4 pentadiol. In two weeks, single orthorhombic crystals (0.25 × 0.1 × 0.04 mm) appeared. From the cryo-cooled crystal, X-ray diffraction data were collected on beamline 5C at the Pohang Accelerator Laboratory (PAL), South Korea [11]. The crystal was diffracted at 3.2 Å resolution. Data were integrated using DENZO and scaled using SCALEPACK [12]. The statistics on data collection and processing are summarized in Table 1.

Table 1. Data collection and refinement statistics.

Data	<i>XoGroEL</i> (PDB ID: 6KFV)
Data collection	
Wavelength (Å)	0.97949
Resolution range (Å)	47.2–3.2 (3.3–3.2) *
Space group	<i>P2₁2₁2₁</i>
Unit cell (Å)	137.1 239.5 278.3 90 90 90
Total reflections	683,467
Unique reflections	136,180 (10475)
Multiplicity	4.1 (3.0)
Completeness (%)	91.7 (71.3)
Mean I/sigma (I)	8.5 (2.1)
Wilson B-factor	68.9
R-merge	18.9 (59.0)
Refinement	
Reflections used in refinement	136,115 (10,470)
Reflections used for R-free	6839 (542)
R-work	0.21 (0.31)
R-free	0.29 (0.37)
Number of non-hydrogen atoms	
In macromolecules	53,872
In ligands	28
In solvent	33
Protein residues	7342
RMS (bonds)	0.015
RMS (angles)	1.87
Ramachandran favored (%)	82.8
Ramachandran allowed (%)	13.2
Ramachandran outliers (%)	4.0
Rotamer outliers (%)	16.5
Average B-factor	
Macromolecules	82.3
Ligands	99.3
Solvent	36.9

* Values in parentheses are for the shell with the highest resolution. $R_{\text{merge}} = \frac{\sum_{hkl} \sum_i |I_i(hkl) - \langle I(hkl) \rangle|}{\sum_{hkl} \sum_i I_i(hkl)}$, where $I_i(hkl)$ is the mean intensity of *i*th observation of symmetry-related reflections *hkl*. $R_{\text{free}} = \frac{\sum_{hkl} ||F_{\text{obs}}| - |F_{\text{calc}}||}{\sum_{hkl} |F_{\text{obs}}|}$, where F_{calc} is the calculated protein structure factor from the atomic model (R_{free} was calculated with a randomly selected 5% of the reflections).

2.4. Structure Determination

Phases of *XoGroEL* were determined by molecular replacement (MR) with Phaser in the CCP4 software package (Oxon, UK) [13] using *E. coli GroEL* (PDB ID: 4PKN [14], 78% sequence identity) as the search model. Model building and electron density interpretations were carried out using the COOT program (Oxford, UK) [15]. Structure was refined using the CCP4 program Refmac5 [16]. Structure was validated using WHATIF [17] and SFCHECK [18]. The determined *XoGroEL* structure was deposited in PDB (PDB ID: 6KFV). The refinement statistics are shown in Table 1. Graphical representations were created using PyMOL (New York, NY) [19].

3. Results

3.1. Molecular Packing of *XoGroEL* in Crystal

There were 14 protomers in the asymmetric unit of *XoGroEL* crystal. The space group was determined as *P2₁2₁2₁* as there were three two-fold screw crystallographic axes along the unit cell axes of **a**, **b**, and **c** (Figure 1). The 14 protomers existed as two rings; one ring consisted of seven protomers and was stacked back-to-back on the other ring. The stacking axis was parallel to the longest axis **c**.

XoGroEL of 14 protomers was also stacked on other *XoGroEL* molecule in a staggered way. Each ring was in contact with six other symmetry-related rings parallelly in $a \times b$ plane like a flower-shape.

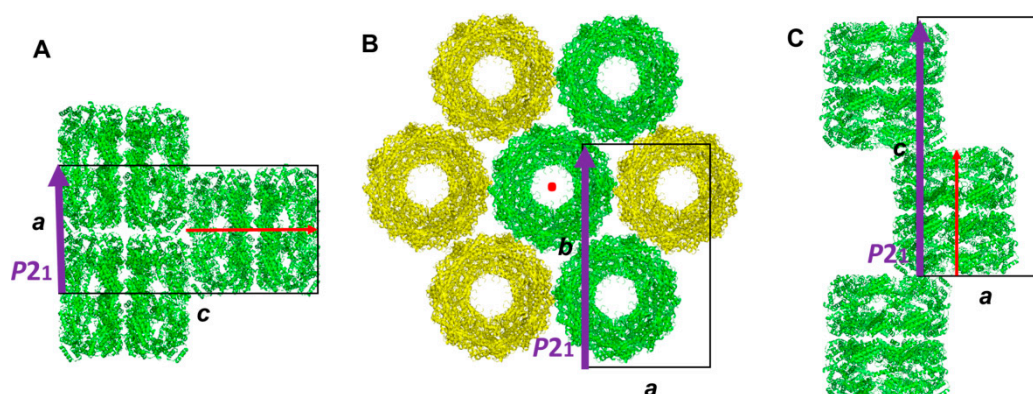


Figure 1. Symmetry-related *XoGroEL* molecules in unit cell. *XoGroEL* molecules in $P2_1$ symmetry along with a axis in $a \times c$ plane (A), along with b axis in $a \times b$ plane (B), and along with c axis in $a \times c$ plane (C). Two-fold screw axis of $P2_1$ is represented as purple arrows. Stacking axis of two homoheptameric rings in *XoGroEL* is represented as red arrows. A red arrow perpendicular to $a \times b$ plane is shown as red dot in (B).

3.2. Overall Structure of *XoGroEL*

The *XoGroEL* consisted of 14 protomers, arranged in a symmetry as two back-to-back seven-member rings (Figure 2A,B). Each *XoGroEL* protomer was composed of three domains of an equatorial domain at the back-to-back interacting surface between rings, an apical domain at the terminal ends, and an intermediate domain connecting the equatorial and apical domains (Figure 2C, Figures S1 and S2). Two rings were in contact each other in a staggered way at equatorial domains. There was an ATP-binding pocket in each equatorial domain. ATP binding and hydrolysis is known to cause major movements during the reaction cycle of substrate protein folding (Figure 2D). Apical domain existed at the terminal end of the cylinder and exposed hydrophobic residues to solvent facing the internal cavity of substrate protein binding pocket.

3.3. Conformation of *XoGroEL* Protomer

GroEL undergoes a series of conformational changes during the cycle of substrate protein folding with co-chaperone *GroES* and ATP [9] (Figure 2D). The traditional “bullet cycle” model proposes that the binding of ATP and substrate unfolded protein facilitates *GroES* binding to *GroEL*, which encapsulates a folding chamber of the cis ring. After the hydrolysis of bound ATP in the cis ring, ATP binding in the opposite trans ring releases folded protein from the cis ring and initiates a new cycle of unfolded protein of *GroEL* [20].

When the 14 protomers of *XoGroEL* were structurally compared to each other, the conformation of each protomer was well conserved. The root mean square deviation (RMSD) between *XoGroEL* protomers was less than 0.85 Å in more than 400 amino acids. *XoGroEL* structure was superimposed to the Apo structure (PDB ID: 1XCK [21]) and *GroES* and ATP-bound structure (PDB ID: 3WVL [22]) of *E. coli GroEL* (*EcGroEL*). *XoGroEL* was well superimposed to the open form of apo *EcGroEL* with RMSD of 0.77 Å in 481 amino acids (Figure 3A). In the open form of *GroEL*, protomers in the cis ring and in the trans ring had the same conformation. When *GroEL* bound to ATP and *GroES*, *GroEL* had an allosteric conformational change of both apical and intermediate domains (Figure 3B). The apical domain moved away from the equatorial domain, and the intermediate domain got closer to the equatorial domain to form a tight ATP-binding site.

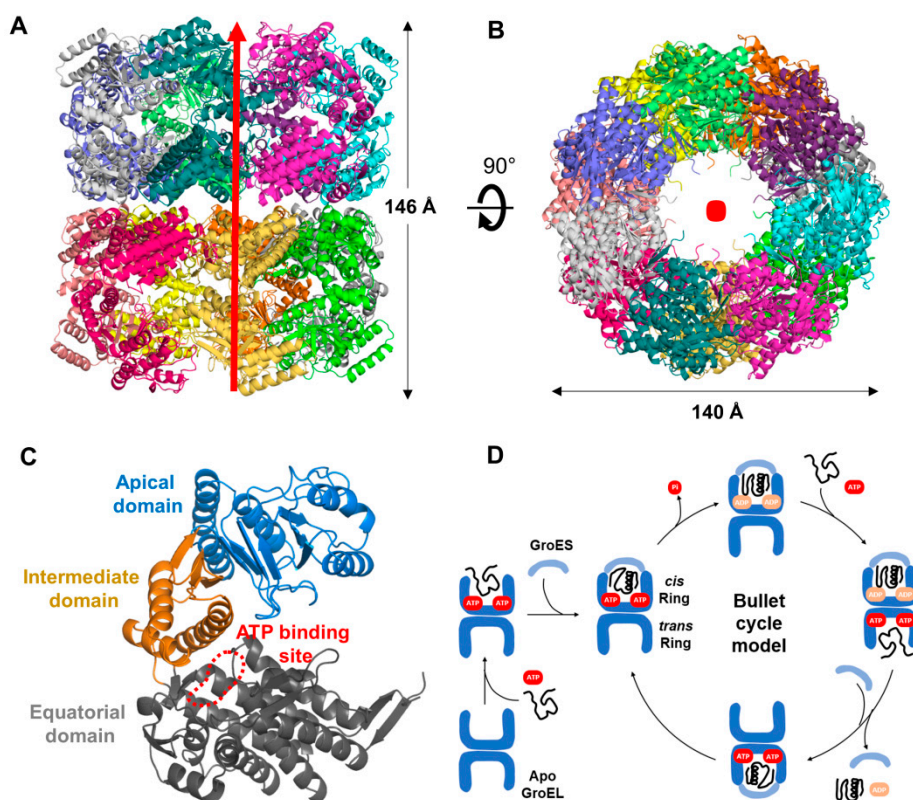


Figure 2. Crystal structure and mechanism of *XoGroEL*. *XoGroEL* structure with 14 protomers from side view (A) and top view (B). Red arrow and red dot represent the stacking axis of two homoheptameric rings in *XoGroEL*. (C) Apical (pale blue), intermediate (orange), and equatorial (grey) domains with ATP-binding site (red dotted line) in a *XoGroEL* protomer. (D) A bullet cycle model of chaperonin *GroEL* and co-chaperonin *GroES* (modified from [9]).

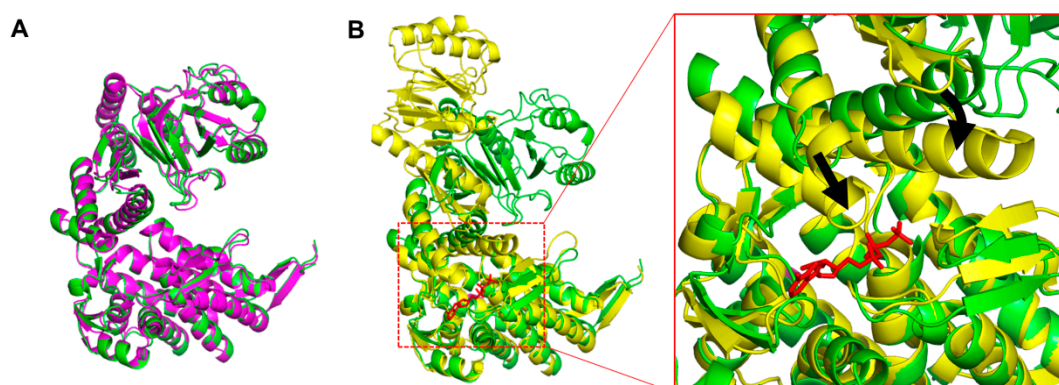


Figure 3. Conformation of *XoGroEL* protomer. (A) Superimposed structures of an open form of *XoGroEL* (green) and *EcGroEL* (purple). (B) Superimposed structures of an open form of *XoGroEL* (green) and a closed form of *EcGroEL* (yellow) in complex with ATP (red) and *GroES* (not shown in this figure). The conformational change on ATP binding in the intermediate domain is shown by the black arrow.

Although we tried to determine *XoGroES* (*GroES* from *Xoo*) or ATP-bound *XoGroEL* structure with a soaking method, we could not determine the complex structure. In the *XoGroEL* crystal packing, there was no free space above the cis ring of *XoGroEL* for *XoGroES* binding. The tight packing between *XoGroEL* molecules also prohibited the conformational change of the apical and equatorial domains caused by ATP binding in the *XoGroEL* crystal. We could not get the cocrystallization condition for ATP-bound *XoGroEL* or *XoGroES*-bound *XoGroEL*.

4. Discussion

A protomer of *XoGroEL* consists of 546 amino acids (57 kDa). Fourteen protomers of *XoGroEL* constitute a large complex of more than 800 kDa. Although various approaches for the crystallization of a mega Dalton protein complex have been developed [23,24], the determination of the crystal structure of such a large complex at high quality is still challenging. The overall B factor (temperature factor) of *XoGroEL* is 82.3. Conformation of each protomer of *GroEL* changes allosterically upon the binding of substrate unfolded protein, ATP, and *GroES* during catalysis. We speculate the high B factor comes from the flexible conformation of *XoGroEL* in the open form before substrate binding. When we analyzed the B factor of the *XoGroEL* structure by domain, the equatorial domain, located at the interface between two homoheptameric rings, had the lower average B factor of 62.6, while the intermediate domain had 88.7 and the apical domain had 104.0 (Figure S1). With the current X-ray diffraction data, the electron density for the side chain of residues was weak, especially in the apical domain, which caused approximately 8% of the difference between R-work and R-free values. In the open form of *XoGroEL* without *XoGroES* and ATP binding, the apical domain to bind substrate unfolded protein seemed to be more flexible than the equatorial domain.

We used the previously published RNASeq data to study the time-resolved transcriptional expressions of *XoGroEL/XoGroES* genes in the pathogenicity activated (rice leaf extract-treated) and control (untreated) *Xoo* cells [25]. The RNASeq data were obtained from in vitro assay system to activate the pathogenicity of *Xoo* cells by treating rice leaf extract on the *Xoo* cell culture. The in vitro assay system enabled us to simultaneously initiate the pathogenicity of *Xoo* cells in the culture broth, which provided a high signal-to-noise transcriptome data compared to in vivo data. Both *XoGroEL* and *XoGroES* genes showed the U-shaped gene expression pattern in the first hour, i.e., the decreased expression in the initial 30 min (approximately 50%) and the recovered expression in an hour (Figure S3). Although transcriptional expression patterns and expression level fold changes of *GroEL* and *GroES* genes were similar, the *GroEL* gene had three times higher RPKM value than the *GroES* gene. The RNASeq data showed that, at the initial stage of *Xoo* and rice interaction, both *XoGroEL* and *XoGroES* genes were downregulated and recovered to the normal expression level in an hour. The crystal structure and pathogenicity-related expression of *XoGroEL* will provide better understanding of the chaperone function of *Xoo* in pathogenicity.

Supplementary Materials: The following are available online at <http://www.mdpi.com/2073-4352/9/8/399/s1>, Figure S1: The B factor of *XoGroEL* protomers in crystal and the 2FoFc map of *XoGroEL* protomer, Figure S2: The sequence alignment of chaperonin *GroELs*, Figure S3: Time-resolved transcriptional expression of *XoGroEL* (*Xoo4288*) and *XoGroES* genes (*Xoo4289*) of *Xoo* on rice leaf extract (RLX) treatment.

Author Contributions: T.H.T. and L.J. planned and preformed the experiments, analyzed the data, and wrote the manuscript. P.H. and A.Y.J. analyzed the data and wrote the manuscript. K.S. and K.J.G. preformed the RNASeq analysis.

Funding: This work was carried out with the support of the "Cooperative Research Program for Agriculture Science & Technology Development" (Project No. PJ013270012019), Rural Development Administration, Republic of Korea, the project "Development of biomedical materials based on marine proteins" (Project No. 20170305), funded by the Ministry of Oceans and Fisheries, Korea (J.-H.L.), and the Bio & Medical Technology Development Program of the National Research Foundation of Korea (NRF) funded by the Ministry of Science and ICT (NRF-2017M3A9E4078017).

Acknowledgments: We are grateful to the staff members of Beamline 5C at the Pohang Accelerator Laboratory (PAL), Korea.

Conflicts of Interest: The authors declare no conflict of interest.

References

1. FAOSTAT. Available online: <http://faostat.fao.org> (accessed on 1 August 2019).
2. Khush, G.S. What it will take to feed 5.0 billion rice consumers in 2030. *Plant Mol. Biol.* **2005**, *59*, 1–6. [[CrossRef](#)] [[PubMed](#)]
3. Verdier, V.; Vera Cruz, C.; Leach, J.E. Controlling rice bacterial blight in Africa: needs and prospects. *J. Biotechnol.* **2012**, *159*, 320–328. [[CrossRef](#)] [[PubMed](#)]

4. Alfano, J.R.; Collmer, A. Type III secretion system effector proteins: Double agents in bacterial disease and plant defense. *Annu. Rev. Phytopathol.* **2004**, *42*, 385–414. [[CrossRef](#)] [[PubMed](#)]
5. Nans, A.; Kudryashev, M.; Saibil, H.R.; Hayward, R.D. Structure of a bacterial type III secretion system in contact with a host membrane in situ. *Nat. Commun.* **2015**, *6*, 10114. [[CrossRef](#)] [[PubMed](#)]
6. Portaliou, A.G.; Tsolis, K.C.; Loos, M.S.; Zorzini, V.; Economou, A. Type III secretion: Building and operating a remarkable nanomachine. *Trends Biochem. Sci.* **2016**, *41*, 175–189. [[CrossRef](#)] [[PubMed](#)]
7. Parsot, C.; Hamiaux, C.; Page, A.L. The various and varying roles of specific chaperones in type III secretion systems. *Curr. Opin. Microbiol.* **2003**, *6*, 7–14. [[CrossRef](#)]
8. Hartl, F.U.; Bracher, A.; Hayer-Hartl, M. Molecular chaperones in protein folding and proteostasis. *Nature* **2011**, *475*, 324–332. [[CrossRef](#)]
9. Skjaerven, L.; Cuellar, J.; Martinez, A.; Valpuesta, J.M. Dynamics, flexibility, and allostery in molecular chaperonins. *FEBS Lett.* **2015**, *589*, 2522–2532. [[CrossRef](#)]
10. Tran, H.T.; Pham, T.V.; Ngo, H.P.; Hong, M.K.; Kim, J.G.; Lee, S.H.; Ahn, Y.J.; Kang, L.W. Crystallization and preliminary X-ray crystallographic analysis of the *XoGroEL* chaperonin from *Xanthomonas oryzae* pv. *oryzae*. *Acta Crystallogr. F Struct. Biol. Commun.* **2014**, *70*, 604–607. [[CrossRef](#)]
11. Park, S.Y.; Ha, S.C.; Kim, Y.G. The protein crystallography beamlines at the pohang light source II. *Biodesign* **2017**, *5*, 30–34.
12. Otwinowski, Z.; Minor, W. Processing of X-ray diffraction data collected in oscillation mode. *Meth. Enzymol.* **1997**, *277*, 307–326.
13. McCoy, A.J.; Grosse-Kunstleve, R.W.; Adams, P.D.; Winn, M.D.; Storoni, L.C.; Read, R.J. Phaser crystallographic software. *J. Appl. Crystallogr.* **2007**, *40*, 658–674. [[CrossRef](#)] [[PubMed](#)]
14. Fei, X.; Ye, X.; LaRonde, N.A.; Lorimer, G.H. Formation and structures of *GroEL*: *GroES2* chaperonin footballs, the protein-folding functional form. *Proc. Natl. Acad. Sci. USA* **2014**, *111*, 12775–12780. [[CrossRef](#)] [[PubMed](#)]
15. Moodie, E.E.; Richardson, T.S.; Stephens, D.A. Demystifying optimal dynamic treatment regimes. *Biometrics* **2007**, *63*, 447–455. [[CrossRef](#)] [[PubMed](#)]
16. Mansell, W. An integrative formulation-based cognitive treatment of bipolar disorders: Application and illustration. *J. Clin. Psychol.* **2007**, *63*, 447–461. [[CrossRef](#)] [[PubMed](#)]
17. DeFrank, J.J.; Cheng, T.C. Purification and properties of an organophosphorus acid anhydrase from a halophilic bacterial isolate. *J. Bacteriol.* **1991**, *173*, 1938–1943. [[CrossRef](#)]
18. Steegborn, C.; Messerschmidt, A.; Laber, B.; Streber, W.; Huber, R.; Clausen, T. The crystal structure of cystathionine gamma-synthase from nicotiana tabacum reveals its substrate and reaction specificity. *J. Mol. Biol.* **1999**, *290*, 983–996. [[CrossRef](#)]
19. DeLano, W.L. *The PyMOL Molecular Graphics System*; Version 1.3r1; Schrodinger: New York, NY, USA, 2010.
20. Clare, D.K.; Vasishtan, D.; Stagg, S.; Quispe, J.; Farr, G.W.; Topf, M.; Horwich, A.L.; Saibil, H.R. ATP-triggered conformational changes delineate substrate-binding and -folding mechanics of the *GroEL* chaperonin. *Cell* **2012**, *149*, 113–123. [[CrossRef](#)]
21. Bartolucci, C.; Lamba, D.; Grazulis, S.; Manakova, E.; Heumann, H. Crystal structure of wild-type chaperonin *GroEL*. *J. Mol. Biol.* **2005**, *354*, 940–951. [[CrossRef](#)]
22. Koike-Takeshita, A.; Arakawa, T.; Taguchi, H.; Shimamura, T. Crystal structure of a symmetric football-shaped *GroEL*: *GroES2*-ATP14 complex determined at 3.8Å reveals rearrangement between two *GroEL* rings. *J. Mol. Biol.* **2014**, *426*, 3634–3641. [[CrossRef](#)]
23. Govada, L.; Chayen, N.E. Choosing the method of crystallization to obtain optimal results. *Crystals* **2019**, *9*, 106. [[CrossRef](#)]
24. Blackburn, A.; Partowmah, S.H.; Brennan, H.M.; Mestizo, K.E.; Stivala, C.D.; Petreczky, J.; Perez, A.; Horn, A.; McSweeney, S.; Soares, A.S. A simple technique to improve microcrystals using gel exclusion of nucleation inducing elements. *Crystals* **2018**, *8*, 464. [[CrossRef](#)]
25. Kim, S.; Cho, Y.J.; Song, E.S.; Lee, S.H.; Kim, J.G.; Kang, L.W. Time-resolved pathogenic gene expression analysis of the plant pathogen *Xanthomonas oryzae* pv. *oryzae*. *BMC Genom.* **2016**, *17*, 345. [[CrossRef](#)] [[PubMed](#)]

